# CHAPTER 6

# MANUFACTURING ORIGAMI STENT GRAFT

This chapter deals with the manufacture of the novel origami stent graft based on geometric parameters derived earlier in this dissertation. At present most existing stents and stent grafts are made from stainless steel and TiNi shape memory alloy (SMA). The same materials will be used to produce the new stent graft here. Stents currently in production use these materials in a wire form. Rather than the wire form this chapter describes the use of these materials in sheet form, which can be easily manufactured into a tubular shape for the stent graft. A photochemical etching technique was used to engrave folds into the materials.

The main advantage of using SMA sheet is that it is possible to make a stent graft which can self-expand to the desired shape at body temperature without the use of an expansion tool. However, SMA sheet is a relatively new material and the applications are still limited. Therefore, processing techniques including photochemical etching and heat-treatment of SMA sheet need to be established.

Section 6.1 explains how a stainless steel sheet can be used to make the novel origami stent graft. Section 6.2 deals with the etching and heat-treatment processing of the TiNi SMA sheet. Sections 6.3 and 6.4 demonstrate models of the new stent grafts produced with Ti-rich and Ni-rich TiNi SMA sheets as well as illustrations of the self-expansion of the stent grafts.

The models produced here are the same size as standard oesophageal and aortal stent grafts.

## 6.1 Foldable cylindrical tubes using a stainless steel sheet

The stainless steel sheet 316L is used to make the stent graft. The desirable patterns of grooves for folds can be created on the sheet using a conventional negative etching technique (Allen 1986). The depth of the grooves can be controlled by the length of etching time. After etching the sheet is rolled into a tube. The etched grooves act as hinges when the tube is folded.

Figures 6.1(a) and (b) show part of the pattern of folds for the front and reverse sides of the sheet, which correspond to the outer and inner surfaces of the foldable cylindrical tube. This is the same pattern described in the stent graft of Chapter 3 where $\alpha_1 = \alpha_2 = 45^o$. The size of the sheet is 100 mm x 110 mm x 0.08 mm. The thickness of the sheet is the same as the thickness of the cover on currently produced stent grafts. The pattern of folds consists of square elements with sides of length 10 mm. The number of elements in both vertical and longitudinal directions are 8. The width of the grooves is 1.2 mm. These values are selected to produce a stent graft, as mentioned previously, that is useful for oesophageal and aortal conditions.

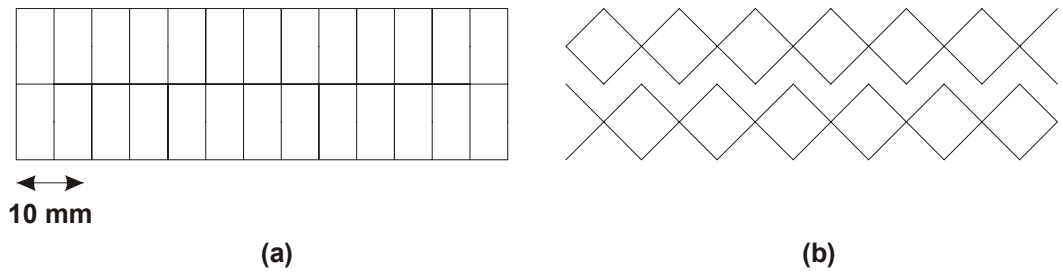


**Figure 6.1 (a) Folding pattern of outer surface and (b) inner surface of the foldable cylindrical tube.**

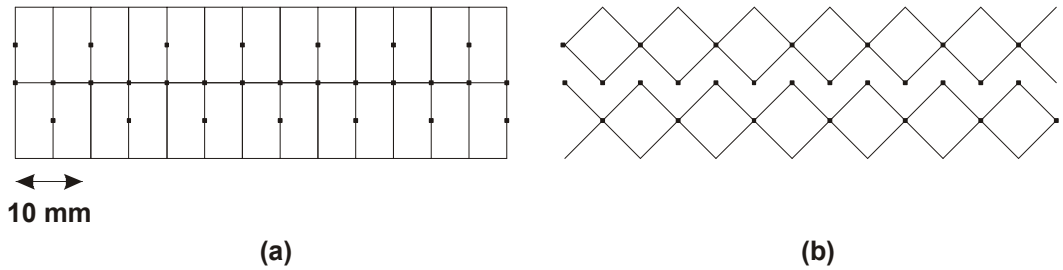


**Figure 6.2 Folding pattern with squares hole on (a) outer surface and (b) inner surface of the foldable cylindrical tube.**

Figure 6.2 shows a slightly different pattern of folds. In this pattern, holes are placed at each line intersection. These holes have a square shape. The positions of holes on the front and reverse sides of the sheet coincided, so they become through-holes. The holes help to alleviate high concentrations of stress when the sheet is folded. The length of the sides of the elements is again 10 mm. The width of folding lines is 0.5 mm, and the size of each hole is 0.5 mm x 0.5 mm. It is also possible to use circular holes.

These patterns were first stenciled on, and then both sides of the sheet were etched at the same time. The etching depth was half of the thickness of the sheet, which was 0.04 mm. After etching, the sheet was rolled and joined together by glue to form a cylindrical tube. The tube was folded manually.

Photographs of the foldable cylindrical tubes for the origami stent graft without and with holes in both its fully folded and expanded configurations are shown in Figures 6.3 - 6.5. The grooves created by etching outside and inside of the tubes became peak and trough creases, respectively. The foldable cylindrical tube with helical folds has also been produced successfully as shown in Figure 6.5.

Figure 6.3(b) shows a close-up photograph of the folds without holes and the folds width was 1.2 mm. As indicated in the photograph, some of the folds were distorted or improperly folded. Therefore, it seems that it might not be suitable to use a wider groove.

For the model shown in Figure 6.4 the radius and length of the foldable cylindrical tube before folding are 12.5 mm and 80 mm, respectively. The radius and length of the tube in its fully folded configuration are 5 mm and 45 mm, respectively. Thus, the tube is folded radially and longitudinally to about 40% and 56% of the original dimensions of the tube. These numbers could be smaller if the foldable cylindrical tube was designed with a large number of the elements as described in Chapter3.

Folding of the cylindrical tubes shown in Figures 6.3 - 6.5 is easily accomplished by first applying a small pressure to the intersections of the grooves as shown in Figure 6.6. This sets up the preferred direction of deformation. Then the tube is compressed in the longitudinal direction, and the stent graft is compressed to its fully folded configuration. For the tubes with helical lines the structure is twisted as well as compressed. This process causes all parts of the tube to collapse together instantly so that we do not need to fold each of the folds individually.

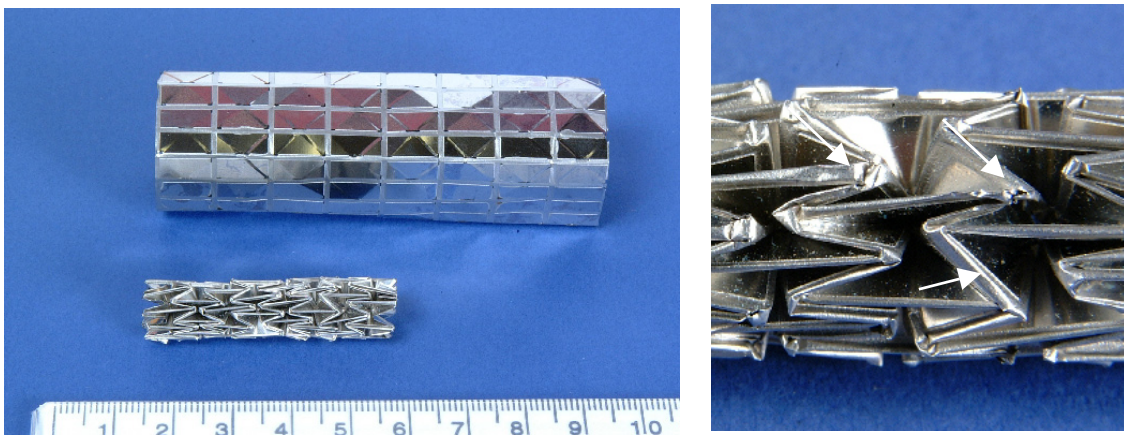

**(a)** **(b)**

**Figure 6.3 (a) Cylindrical tube with 1.2 mm width folds in its fully folded and expanded configurations and (b) close up view of the folds.**

(a)

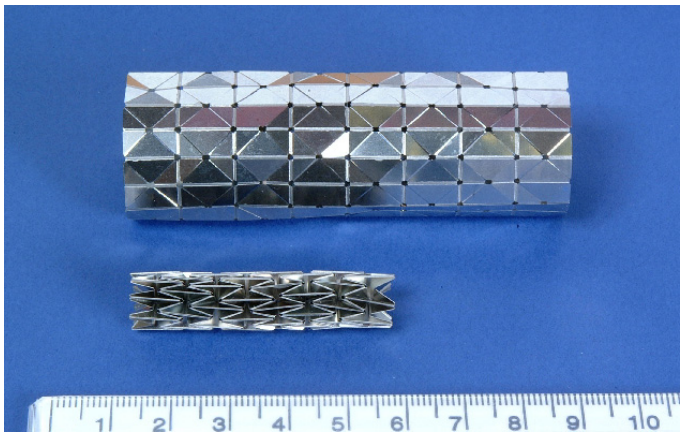

(b)

**Figure 6.4 Cylindrical tube with 0.5 mm width folds in its fully folded and expanded configurations at (a) end and (b) perspective views.**
**The folding pattern contains holes at the intersections of folds.**

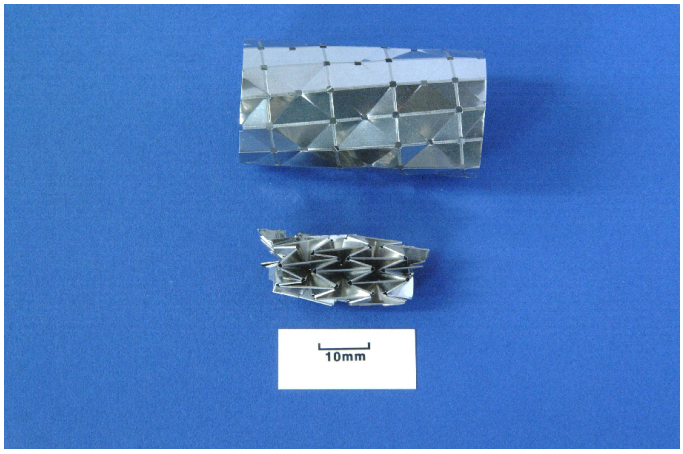


**Figure 6.5 Stent graft with helical folds in its fully folded and deployed configurations.**
**Again holes exist in the folding pattern.**

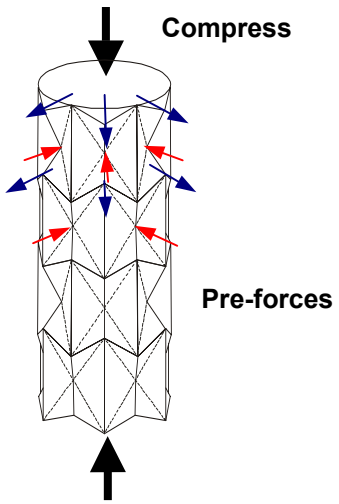


**Figure 6.6 Forces in radial and longitudinal directions are applied to aid the folding of the stent graft.**

The results above prove that the novel origami stent grafts can be produced using metals, and presumably any similar biocompatible materials. However the stainless steel stent graft was fairly rigid when deployed. Using different biocompatible materials such as polyester, PTFE or stainless steel of reduced density would improve flexibility.

In these prototypes, glue is used to connect the ends of the sheet to form a cylindrical tube. Spot welding may also be used. In the future it may be more appropriate to produce the stent graft using a tube instead of a sheet. However, to produce the grooves inside of a tube may be complicated.

The folding process required to fold the stent graft could be initiated using a mechanical method such as a press. The use of a press to create an uneven pattern on the surface of a drinking can has been experimented with and used successfully by Miura (2002). This same method would conceivably work well in the automatic folding of the metallic stent.

## 6.2 Processing techniques of shape memory alloy sheet

As mentioned in Chapter 2, there are many potential advantages given by the use of SMA for the stent graft. The biggest advantage is that a stent graft can self-expand to a pre-determined shape by body heat. The main difference between existing SMA stent grafts and the stent graft presented here is that the latter is made using a sheet rather than a wire. This is the first time that a stent has been manufactured using SMA in sheet form.

In this section, processing techniques of a SMA sheet including photochemical etching and heat-treatment are investigated to produce an origami stent graft.

### 6.2.1 Method of etching

The etching technique applied here is based on photochemical etching for the microstructures of thin SMA film described in Chapter 2. SMA is one of the most difficult materials to etch so that a key challenge here is to determine a useable combination of photoresist, etchant materials and processes.

TiNi SMA sheet can be etched using either positive or negative photochemical etching processes. Positive etching is a reliable technique, although the advantage of negative etching is that the etching process is easier and cheaper than positive etching (Allen 1986). Table 6.1 gives a summary of the positive and negative photochemical etching processes.

We adopted both processes for a 0.08 mm thick Ti-rich (Ti-49.8 at%Ni) TiNi sheet. Firstly, three types of artwork (etching patterns) were prepared. Figures 6.7(a) and (b) show the designs for the trial positive and negative etching techniques. The white lines on a black background in Figure 6.7(a) and black lines on a white background in Figure 6.7(b) are the stencils which were etched. Five different line widths between 0.1 and 1.4 mm were etched. The lengths of the lines were 10 mm, and the space between them is 3 mm.

Figure 6.7(c) shows the folding pattern of the stent graft on the front and reverse sides of the sheet, which is the same pattern for the stainless steel stent graft shown in Figure 6.2. These are the artworks used for positive etching. The size of the sheet is 100 mm x 50 mm. 50 mm width is the widest SMA sheet which is commercially available. The pattern of the folds consists of square elements of sides 10 mm with central holes of 0.8 mm. The width of the grooves is 0.3 mm. The number of elements in the vertical and longitudinal directions are 8 and 4, respectively. The holes are matched up on the front and back sides of the sheet so that they become through holes.

**Table 6.1 Photochemical etching process of the shape memory alloy sheet with positive and negative photoresists.**

| Positive etching with a liquid photoresist | Negative etching with a dry photoresist |
|---|---|
| **Artwork** | |
| 1. Design patterns of grooves | |
| 2. Print out with photo prism printer (2400 pix) | |
| **Photoresist** | |
| 3. Clean specimen with pumice powder | 3. Clean specimen with pumice powder |
| 3. Dip coat with a positive photoresist of HRP 506 with 30 mm/min – 0.06 mm in thickness | 4. Laminate a negative photoresist of Riston 205 with 0.035 or 0.07 mm in thickness |
| 4. Soft bake at 348K for 30 min | – |
| 5. 2kW UV expose for 60 sec | 5. 2kW UV expose for 15 sec |
| 6. Develop using PLSI | 6. Develop using potassium carbonate |
| 7. Water rinse | 7. Water rinse |
| 8. Hard bake at 393K for 60 min | 8. Hard bake at 363K for 30 min |
| **Etching** | |
| 9. Etch with solution of HF: $HNO_3$: $H_2O$ =1:1:2, 1:1:4 and 1:4:5 | 9. Etch with solution of HF: $HNO_3$: $H_2O$ =1:1:4 |
| 10. Remove photoresist | 10. Remove photoresist |

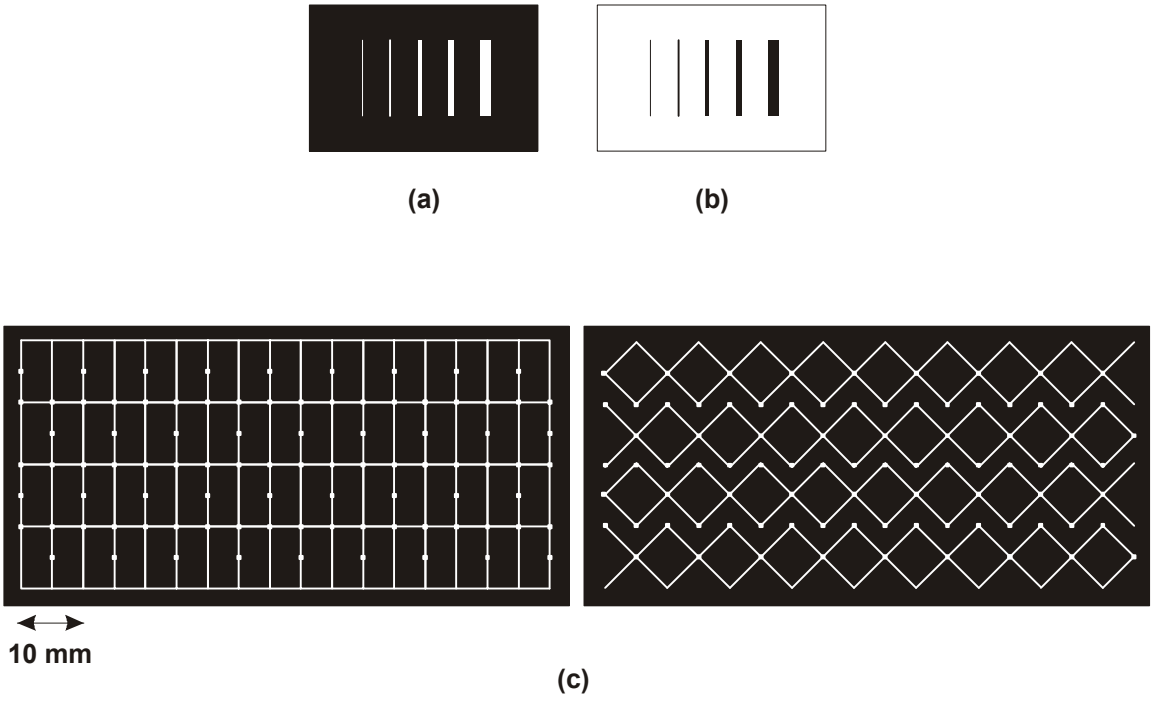


**Figure 6.7 Artworks for the etching pattern with different line widths (0.1, 0.25, 0.5, 0.75 and 1.4 mm) for (a) a positive etching and (b) a negative etching. (c) Positive etching pattern of folds of the origami stent graft on the front and back sides of the sheet.**

After the artwork has been created, the sheet is masked against the chemical etchant by a photoresist. The etchant reacts only on the sheet surface where no photoresist is present, leaving the desired pattern of grooves on the sheet. The photoresist coating must not break down chemically or physically during etching. In order to obtain good adhesion between the sheet surface and the photoresist, the sheet has to be scrubbed clean and abraded using a pumice powder.

For positive etching, a positive-working photoresist (506 Arch Co., USA) was used. It was applied by dip coating, and its thickness could be controlled by the speed of the removal from the dip coater. In this case, the speed was 30 mm/min, which led to a photoresist thickness of 0.006 mm. It is important to make a uniform coating in order to

obtain uniform exposure characteristics. Then, the specimen was soft baked at 348K for 30 minutes to drive off the photoresist solvent from the coating. The pattern was then exposed on the sheet with a 2 kW ultraviolet (UV) light for 60 seconds. It was then developed in a developer with a mixture of 5% trisodium phosphate and 0.75% sodium metasilicate (PLSI Arch, USA) to form a stencil of the pattern on the surface. After that, it was baked at 393 K for 60 minutes to ensure complete drying and to enable the photoresist stencil to toughen.

For negative etching, the specimen was coated with either single or double layers (0.035 mm or 0.070 mm in thickness) by a negative dry photoresist (Riston 205, Dupont Co.). For a negative photoresist, soft baking is not required before the exposure of the UV. The specimen was exposed to a 2 kW UV source for 15 seconds. Then it was developed in a 1% solution of potassium carbonate, and baked at 363 K for 30 minutes.

Finally, the sheet was etched. The etchant is also chosen according to the sheet material. In this experiment the etchant contains mixed solutions of $HF/HNO_3/H_2O$ for both the positive and negative etching processes. To check the effect of the ratio of $HF/HNO_3$ in the solution, an etchant of $HF:HNO_3:H_2O$ in different proportions 1:4:5, 1:1:2 and 1:1:4 by volume were applied. The etchant was carefully mixed in a plastic container in the following order:

1. Prepare the correct quantity of $H_2O$;
2. Prepare the correct quantity of HF;
3. Combine HF to $H_2O$ gently;
4. Prepare the correct quantity of $HNO_3$;
5. Combine $HNO_3$ to $H_2O$ + HF gently.

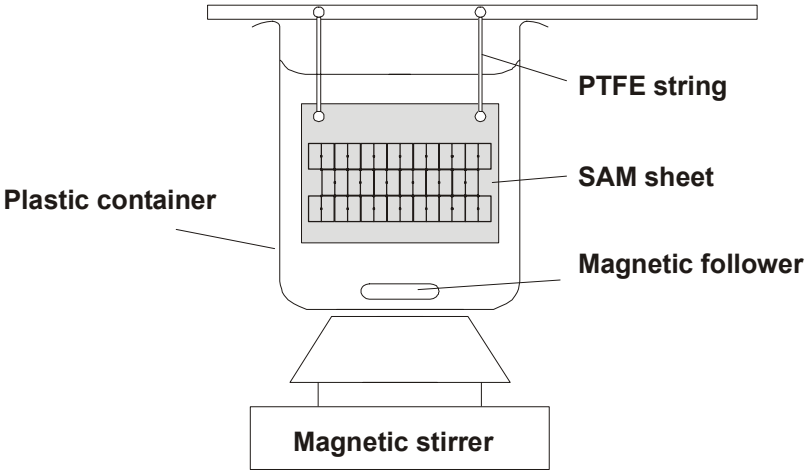


**Figure 6.8 Layout of the etching apparatus.**

The layout of the etching apparatus is illustrated in Figure 6.8. The etchant was kept at 291K and was stirred slowly to create uniform etching. The sheet was held by strings composed of PTFE.

The sheets to test different lines widths shown in Figure 6.7(a) and (b) were etched until of a sheet thickness of 0.08 mm reduced to half, which was between 3 and 25 minutes. The sheet with the patterns of folds for the origami stent graft shown in Figure 6.7(c) was etched until all central through-holes appeared.

After etching, photographs of the etched SMA sheets were taken using a microscope (Olympus, Japan) to observe the quality and properties of the etched patterns. More detailed information of the etched surface was gained using a Scanning Electron Microscopy (SEM) (JSM-6300, JEPL Co., Japan).

When etching a metal using a liquid etchant, it is etched not only in the depth direction, as desired, but also to the side, which results in the formation of a sidewall under the photoresist known as undercut, *U*, shown in Figure 6.9. As a quantitative description of the shape of the etched recess, the etch factor is defined as follows,

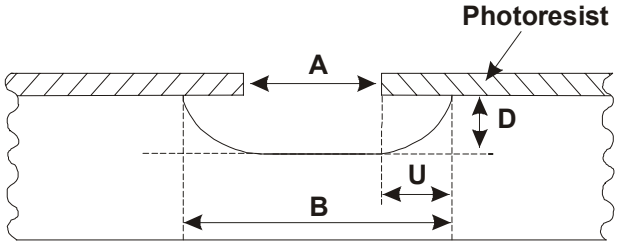


**Figure 6.9 Etch factor = *D*/*U*.**

$$\text{etch factor} = \frac{\text{depth of etch } (D)}{\text{undercut } (U)} \tag{6.1}$$

where undercut $U$ is equal to $1/2(B-A)$. $A$ is the width of the gap in the developed photoresist, and $B$ is the width of the gap that is actually etched. To calculate etch factor and the speed of the etching, the etched depth and width were measured using a surface profiler (Surfometer, Ransducer Technology, UK) and also under the microscope.

The experimental methods described above revealed useful information about the etching process for SMA sheets. This information includes:

- Correct photoresist process, e.g. photoresist type, thickness, UV exposure (intensity and time), and baking temperatures;
- Correct proportion of $HF/HNO_3/H_2O$ of the etchant;
- Etch speed;
- Etch factor.

The results of the experiments are given in Section 6.3.

### 6.2.2 Bending test

The Ti-rich TiNi SMA sheet has a 'rolling' direction which is a result of the cold work that is used to form a flat sheet. The shape memory effect was examined by a bending test to check the effects of bending direction of etched grooves with respect to the rolling direction of the SMA sheet, and the effect of the different groove widths. The bending test was carried out as shown in Figure 6.10. The original shape of the SMA was a flat sheet. A specimen was rolled in a radius $R_0$, and then heated at 393K. The radius of the specimen after heating was denoted as $R$. Photographs were taken before and after bending, and also after heating. $R$ was measured from the photograph. Equations for strain of a bent surface, $\varepsilon$, strain recovery, $\varepsilon_{\text{recovery}}$, and recovery ratio are

$$\varepsilon = \frac{t}{2R_0} \tag{6.2}$$

$$\varepsilon_{\text{recovery}} = \frac{t}{2}\left(\frac{1}{R_0} - \frac{1}{R}\right) \tag{6.3}$$

and

$$\text{Recovery ratio}(\%) = \frac{\varepsilon_{\text{recovery}}}{\varepsilon} \times 100 \tag{6.4}$$

where $t$ is the thickness of the specimen.

Specimens used for this bending test are illustrated in Figure 6.11. The size of the specimens is 5 mm x 30 mm x 0.08 mm. The specimens are cut at $0^o$, $90^o$ and $45^o$ with respect to the rolling direction. The three different groove widths, $w_g$, are 0.3, 0.5 and 0.7 mm. The etching depth, $d$ is 0.04 mm. A negative photochemical etching process was used. The results of these tests are given in Section 6.3.

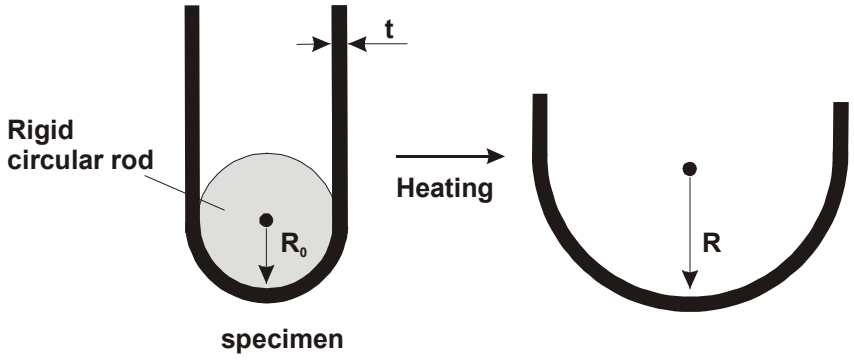


**Figure 6.10 Schematic illustration of the SMA bending test**

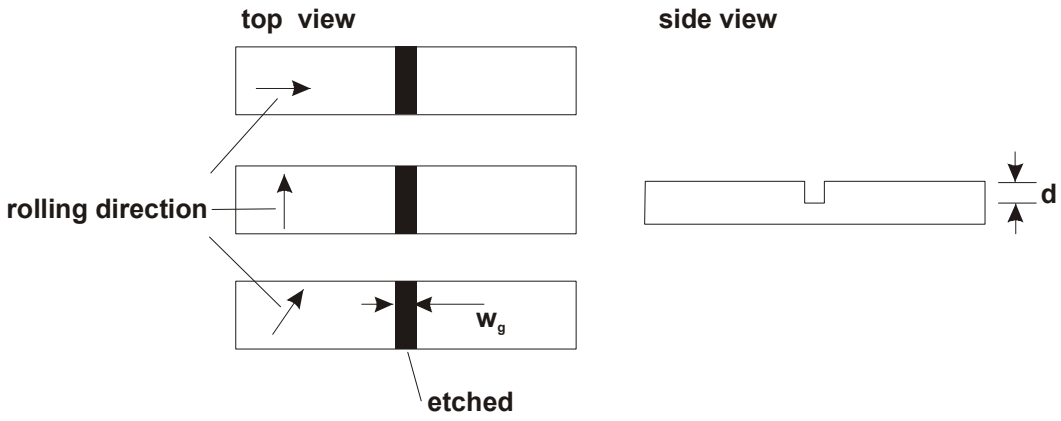


**Figure 6.11 Illustrations of the specimens of Ti-rich SMA sheet with various angles between cuts and the rolling direction, and widths for the bending test.**

### 6.2.3 Heat treatment

In general, the Ti-rich TiNi SMA sheet as supplied cracked when folded due to lack of ductility, making it unsuitable for the production of stent grafts. The SMA sheet was heat-treated to improve its ductility. The 0.08 mm thick Ti-rich TiNi SMA sheet is annealed at 773K for 10 minutes or at 1073K for 1 hour. Annealing at temperature between 773K and 1073K leads to the annihilation of the defects of crystal lattices (dislocations) (Otsuka and Wayman 1998), which are the features giving rise to the resistance to the plastic deformation and therefore cracking. The heat treatment was applied in a vacuum tube (VPC-250F, ULVAC Co) to avoid surface oxidation.

The transformation temperatures before and after treatment are measured by Differential Scanning Calorimetry (DSC) (DSC-8230L, Rigaku Co.) under a flow of argon gas in the temperature range from 473 to 546K with a heating/cooling rate of 0.17 $Ks^{-1}$ to examine the effect of the heat treatment. Then the same bending test described in Section 6.2.2 is carried out to check the characteristic of the shape memory effect after the heat treatment. Again the results of these tests are given in section 6.3.

## 6.3 Results and discussion of the processing technique for SMA

### 6.3.1 Positive etching

The widths of the UV exposed lines of the pattern on the SMA sheets coated with the positive liquid photoresist were measured under a microscope before etching. If the photoresist was over exposed, it was difficult to maintain correct line widths, and if under exposed, there was difficulty developing the image. In this experiment, the error from the original width in the artwork was below 0.03%, implying that the exposure time was correct. Cracking of the photoresist did not occur, which indicated that the baking temperature and time were also correct.

The photoresist peeled off immediately after etching was started with the etchant ratio of $HF:HNO_3:H_2O = 1:4:5$, but it did not peel off when the etchant ratio was either $HF:HNO_3:H_2O = 1:1:4$ or $1:1:2$. Figures 6.12(a) and (b) show photographs taken under a microscope at x5 magnification and cross-sectional profiles of the etched line of 0.5 mm width with different etching times in etchant ratio of $HF:HNO_3:H_2O = 1:1:4$ and $1:1:2$. It took 20 and 10 minutes to etch the pattern of 0.04 mm in depth into the sheets, for the respective $HF:HNO_3:H_2O$ ratios. The dark shadows in the photographs are a consequence of sloping side walls, or undercuts as previously described (see Figure 6.9). As shown in Figure 6.12 in both etchant ratios the undercut of etching increased as the etching time increased. The final size of the etched line and the width of the undercut $U$ are also shown in Figure 6.12. In the case of $HF:HNO_3:H_2O = 1:1:2$, the undercut is about one third smaller than the results in the etchant ratio of $HF:HNO_3:H_2O = 1:1:4$, that is, the etched slope of the side wall of the etched line is steeper and the edge is sharper. However as shown in both the photographs and by the slope of the surface above the undercut in the profiles of Figure 6.12(b), the surface immediately above the undercut is adversely affected by etching and becomes worse as etching progressed.

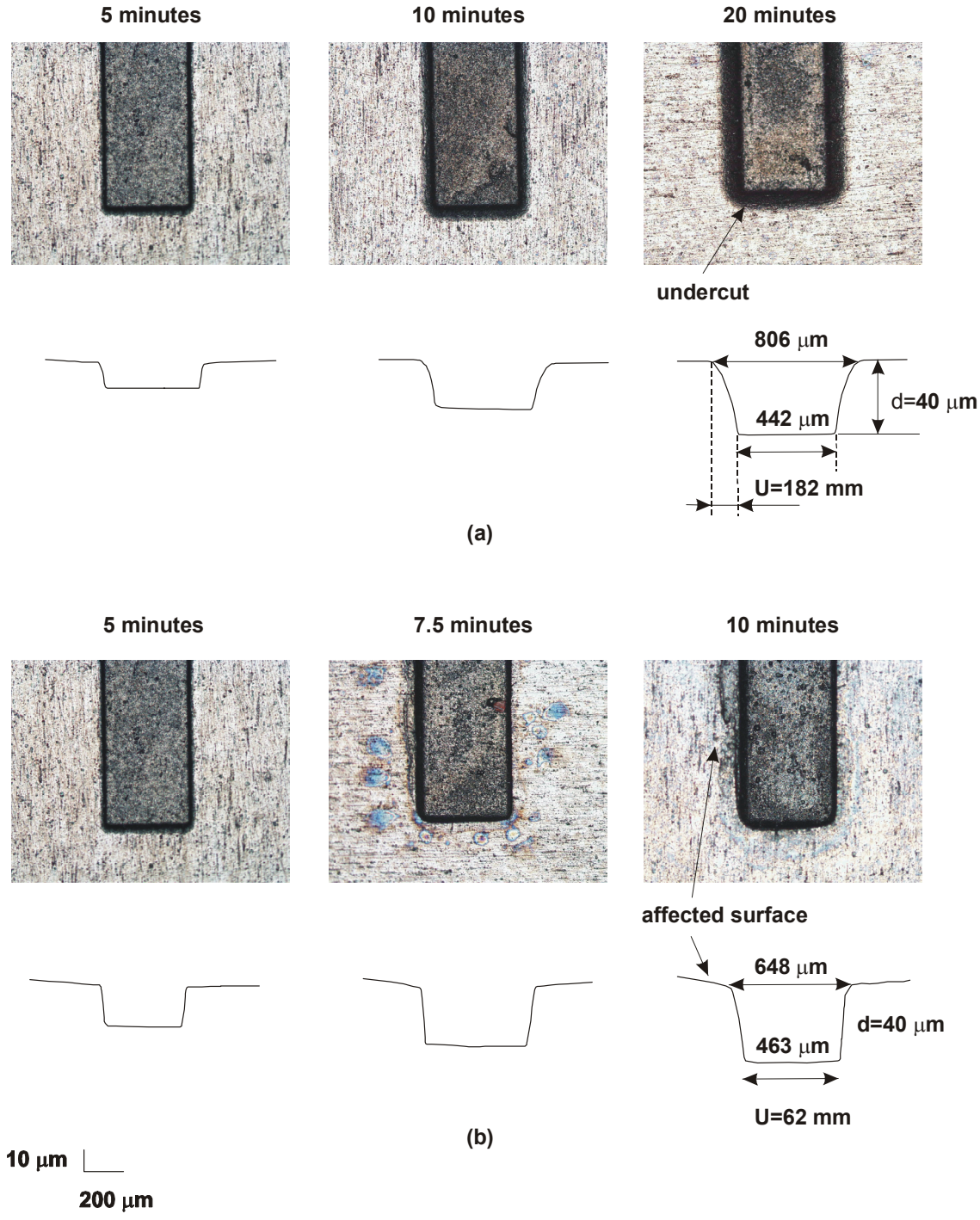


**Figure 6.12 Optical microphotographs and profiles of the etched SMA sheet with a line of 0.5 mm width using the etchant ratio of HF:$HNO_3$:$H_2O$ = (a) 1:1:4 and (b) 1:1:2.**

Further results of the undercut of each of the line widths subjected to etching time in etchant ratio of $HF:HNO_3:H_2O = 1:1:4$ and 1:1:2 are shown in Figure 6.13(a) and (b), respectively. The solid and dashed lines represent an average undercut with the etchant ratio of $HF:HNO_3:H_2O = 1:1:4$ and 1:2:2, respectively. In the case of $HF:HNO_3:H_2O = 1:1:4$, the etching speed of the undercut of wide lines ($\geq 0.75$ mm) is 9.02 μm/min. It is slightly faster than that of narrow lines ($\leq 0.5$ mm) which is 7.79 μm/min. For $HF:HNO_3:H_2O = 1:1:2$, the speed is roughly 4.46 μm/min. The size of the undercut for $HF:HNO_3:H_2O = 1:1:2$ is about two or three times larger than the one for $HF:HNO_3:H_2O = 1:1:4$.

Figure 6.14 shows the results of the etched depth of five different line widths subjected to different etching times. The solid and dashed lines represent an average etching speed with the etchant ratio of $HF:HNO_3:H_2O = 1:1:4$ and 1:2:2, respectively. In the case of $HF:HNO_3:H_2O = 1:1:4$, the etching speed for wide lines ($\geq 0.75$ mm) is 1.7 μm/min, which is slightly faster than the etching speed of narrow lines ($\leq 0.5$ mm) of 1.53 μm/min. Using $HF:HNO_3:H_2O = 1:1:2$, the speed is 3.22 μm/min and there is no difference between different line widths. The depth rate achieved by etching using $HF:HNO_3:H_2O = 1:1:2$ is about twice as fast as the rate for $HF:HNO_3:H_2O = 1:1:4$.

The etch factors of both etchant ratios are calculated using Equation (6.1). Figure 6.15 shows that the etch factors are consistently between 0.2 and 0.3 for $HF:HNO_3:H_2O = 1:1:4$ and range between 0.3 and 0.65 for $HF:HNO_3:H_2O = 1:1:2$.

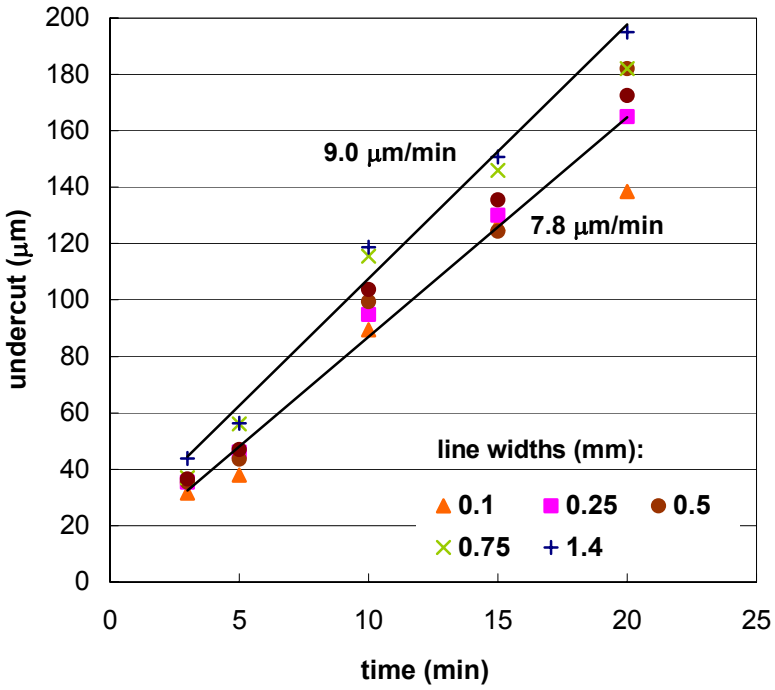


(a)

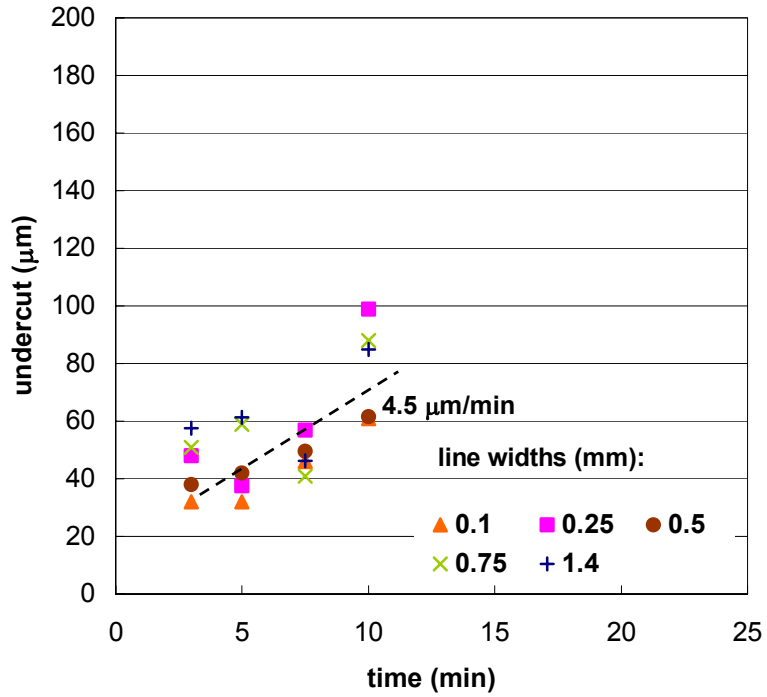


(b)

**Figure 6.13 Change of undercut with time for HF:$HNO_3$:$H_2O$ = (a) 1:1:4 and (b) 1:1:2.**

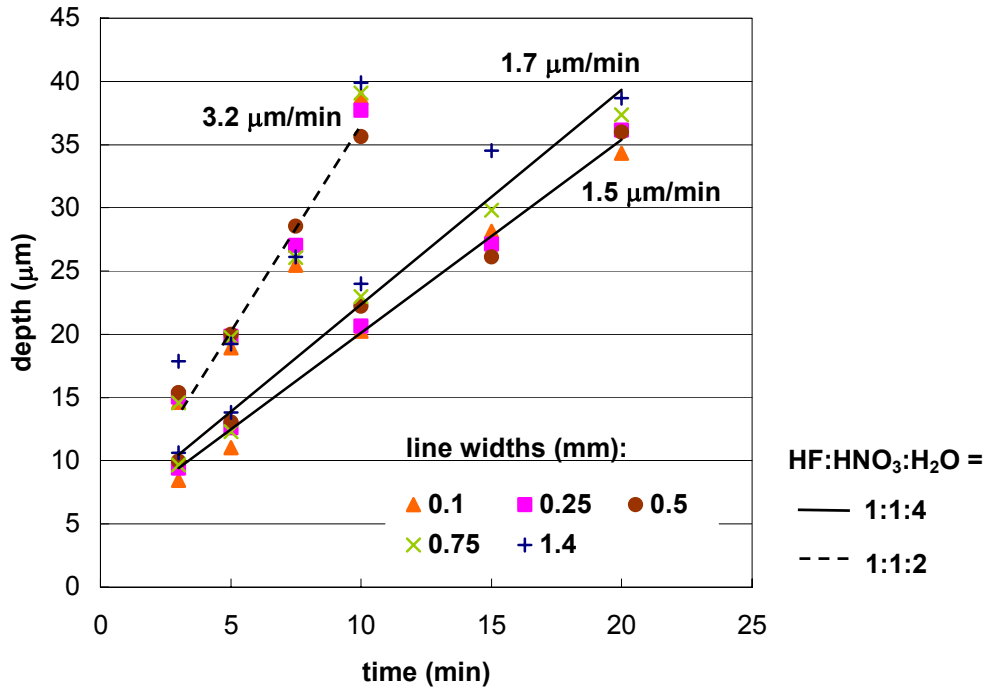


**Figure 6.14 Change of etch depth with time.**

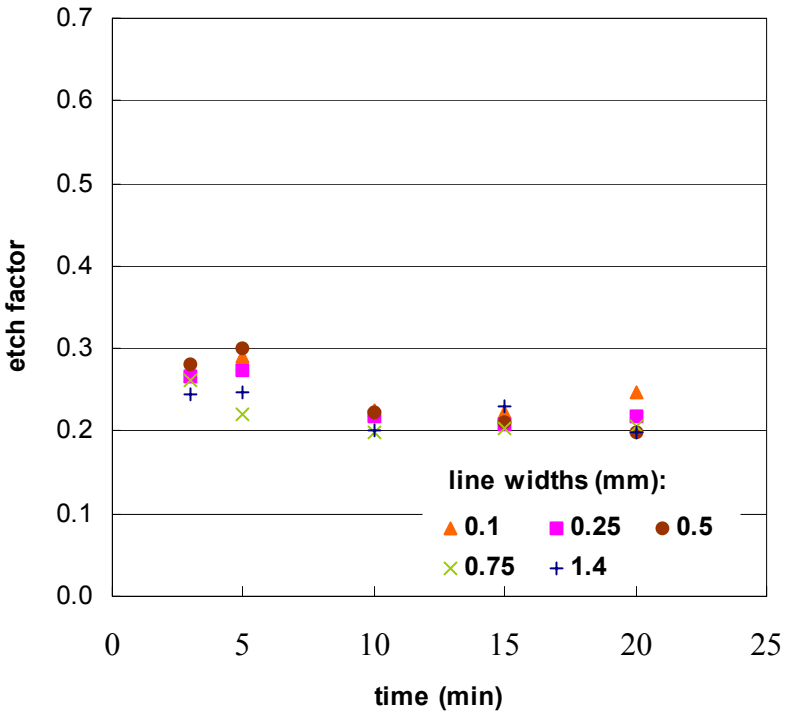


(a)

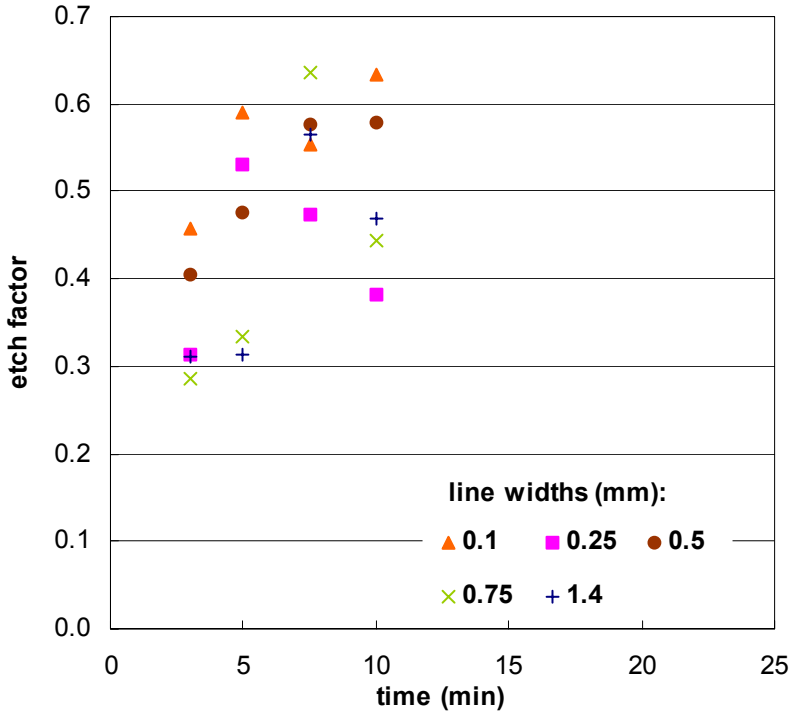


(b)

**Figure 6.15 Etching factor with time when the etchant of $HF:HNO_3:H_2O$ = (a) 1:1:4 and (b) 1:1:2.**

### 6.3.2 Double sided etching using a positive photoresist

The stent pattern shown in Figure 6.7(c) was successfully etched and a good folding pattern was created on a SMA sheet. The total times for all central holes to etch through the sheet are 23 and 10 minutes, for the ratios $HF:HNO_3:H_2O$ = 1:1:4 and 1:1:2 respectively.

Figure 6.16 shows the photographs of the etched Ti-rich TiNi SMA sheets taken under a microscope at x5 magnification just after etching. The photo stencil is still on these sheets. When the etchant ratio $HF:HNO_3:H_2O$=1:1:4 was used the photoresist adhered very well (Figure 6.16a), and the undercut could be seen through the photo stencil. On the other hand, as shown in Figure 6.16(b), using the etchant with higher ratio of $HF/HNO_3$, the photoresist stencil unfortunately came off and the surface above the undercut was affected by etching.

Figure 6.17 shows the photograph of the etched Ti-rich TiNi SMA sheets in $HF:HNO_3:H_2O$=1:1:4 taken under a microscope at x5 magnification after removal of the photoresist. The undercuts of both lines and hole were the same, approximately 0.13 mm. Therefore the etched lines and the size of the hole became 0.56 mm and 1.06 mm, which were 1.87 and 1.34 times their original intended size, respectively.

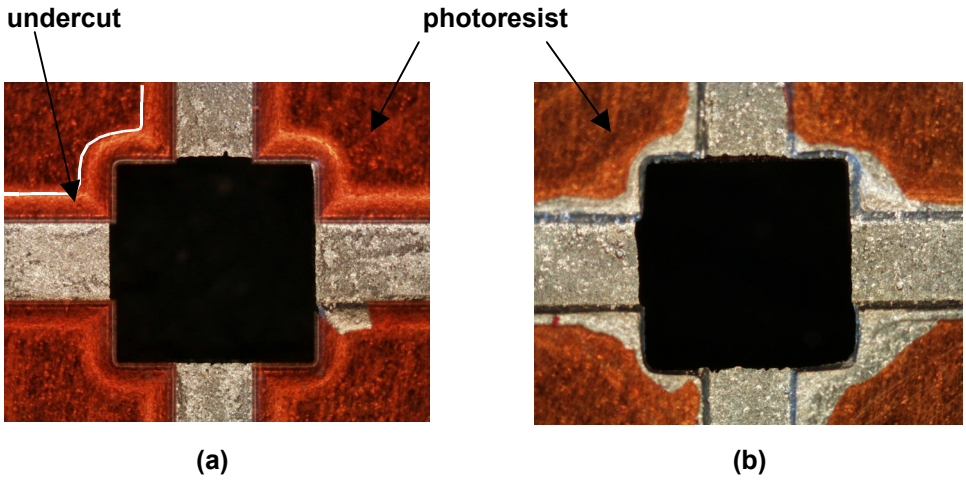


**Figure 6.16 Optical microphotographs of the Ti-rich TiNi SMA sheet etched using the etchant ratio of (a) $HF:HNO_3:H_2O$=1:1:4 and (b) 1:1:2.**